ACCEPTED MANUSCRIPT

Dynamic Deformation Response of Al-Mg and Al-Mg/B_4C Composite at Elevated Temperatures

M. Rezayat[ab], M.H. Parsa[cd*], H. Mirzadeh[c] and J.M. Cabrera[b]

[a]Department of Materials Engineering, Sahand University of Technology, P. O. Box 51335-1996, Tabriz, Iran

[b]Departamento de Ciencia de los Materiales e Ingeniería Metalúrgica, EEBE, Universitat Politècnica de Catalunya, c/Eduard Maristany 10-14, 08019 - Barcelona

[c]School of Metallurgy and Materials Engineering, College of Engineering, University of Tehran, P.O. Box 11155-4563, Tehran, Iran

[d]Center of Excellence for High Performance Materials, School of Metallurgy and Materials Engineering, University of Tehran, Tehran, Iran

*Corresponding Author

Accepted manuscript

Abstract

The dynamic deformations at high temperatures of Al-3wt.%Mg alloy and Al-3wt.%Mg/B_4C composites with different volume fractions and particle sizes were studied using a dilatometer deformation instrument and a split Hopkinson pressure bar operating at strain rates of 10 to 1000 1/s. A comprehensive analytical procedure was developed to correct the effects of adiabatic heating, friction at interface of the specimen and bars, and strain rate variation, on flow stress curves. Then based on corrected data, a physical based constitutive equation was developed for modeling and prediction of flow stress. It was observed that composites in comparison with single phase alloy, after initial straining, showed lower hardening rate which is unexpected. EBSD micrographs and finite element analysis were used to investigate microstructural evolution and deformation condition around particles. It was concluded that particle fracture during deformation which is more expectable in larger particles, and also higher adiabatic heating in composite and not recrystallization related phenomena, are the main reasons for softening of stress flow curves at large deformation.

Keywords*: High temperature dynamic deformation; Constitutive analysis; Microstructural investigation; Flow stress behavior*

ACCEPTED MANUSCRIPT

1. Introduction

Aluminum matrix composites (AMC) as a group of engineering materials have been found various applications in different industries due to their excellent properties [1]. Considering their main fabrication processes, hot deformation has been known as the one of the most important production steps because of their low workability [1]. Generally, deformation at elevated temperatures provides an opportunity to decrease the deformation load, design microstructure and control the final product properties [2]. Addition of Mg as solute in the aluminum matrix of composite, in addition to the improvement of mechanical properties, by hindering the movement of dislocations, reduces the level of recovery as well as increases the stored energy and driving force of dynamic recrystallization (DRX) during high temperature deformation [3,4]. Presence of rigid second phase makes the situation even more complicated because the probability of DRX will be raised by particle stimulating nucleation (PSN). Moreover, the microstructure characteristics including grain size and texture will be also affected [5,6].

Hot deformation of AMCs have been studied at a wide range of strain rates. Most of them have been conducted at strain rates lower that 1 s^{-1} [7,8]; however, strain rates up to 1000 s^{-1} or higher have seldom received attention. In fact, deformation of metals and alloys at high strain rates has been widely studied at low temperatures because it is considered as an interesting subject to unravel the deformation and failure mechanisms in dynamic condition [9,10]. However, the behavior of metal matrix composites (MMC) at high Zener-Hollomon parameters (i.e., relatively low temperature and high strain rates) during high-temperature deformation might be even more interesting, in order to elucidate which are the softening governing mechanisms, whether DRX, dynamic recovery (DRV) or both.

To achieve very high strain rates, split Hopkinson bar systems have been developed. Strain rate in such systems, resulted from a massive and rapid loading via high velocity impact, can be in excess of 1000 s^{-1}. The fluctuations in the initial output signal make the analysis of the flow curves hard [11]. Moreover, the recorded deformation load is only valid for the initial strains, although sample experiences strain until end of the test [12]. Therefore, different constitutive equations including Johnson-Cook [13], Zerilli–Armstrong [14], Hensel–Spittel [15] have been examined to reproduce the suitable flow curves at high strain rates. According to the rate of deformation, adiabatic heating and strain rate variation are unavoidable, and their effects should be corrected to make flow stress curves valid. Therefore, the initial results

Accepted manuscript

ACCEPTED MANUSCRIPT

have unacceptable accuracy and this can limit the application of this deformation technique for studying the hot deformation behavior of engineering materials at high strain rates.

Therefore, the present work aims to quantitative analysis and microstructure evaluation of an Al-3Mg alloy and an Al-3Mg/B_4C composite during high strain rate deformation at elevated temperatures. Moreover, a flow stress correction method is proposed to modify the output of high-temperature split Hopkinson pressure bar test, which considers both adiabatic heating and strain rate variations.

2. Experiment

An Al-3wt.% Mg alloy and an Al-3wt.% Mg/B_4C composite with average particle sizes of 80 and 20 µm and volume fractions of 5, 10, and 15 vol.% were fabricated by stir-casting followed by hot extrusion. Details of materials preparation can be found elsewhere [16]. The chemical composition of the Al-3Mg alloy and the matrix of the composite was evaluated via Electron Probe Micro-Analyzer (Cameca SX100) and Quantometric analysis, respectively. Results indicated a Mg, Fe and Si content as follows: 2.9, 0.15, and 0.2 respectively (in wt.%).

For single-hit hot compression tests at high strain rates, cylindrical specimens with length of 11.5 and 10 mm and diameter of 7.4 and 5 mm were used in a hot split Hopkinson bar test and a deformation dilatometer (Baehr DIL-805), respectively. In hot split Hopkinson bar test deformation was performed at temperature of 300˚C and 400˚C with average strain rate of around 600, 1000 and 1200 s^{-1}. In the deformation dilatometer machine samples were deformed at temperatures of 400 ˚C and 500 ˚C at a strain rate of 10 s^{-1}. Schematic representation of the hot split Hopkinson pressure bar test is shown in Fig. 1a, while the initial and two deformed specimens are presented in and Fig. 1b. The split Hopkinson bar information is presented in Table 1. Electron backscatter diffraction method (EBSD) and Thermal-Field-Emission Scanning Electron Microscope (Jeol 7001f-0.1-30 kV) were employed in order to examine the microstructure of the rapidly quenched (less than 0.5 sec) deformed samples. For this purpose samples were prepared according to standard metallographic procedures. In order to distinguish between high angle grain boundaries (HAGB) and low angle grain boundaries (LAGB) the misoriention of 15° was selected, i.e., grain boundary is considered as HAGB where misorientation is above 15° and considered as LAGB where misorientation is between 3° to 15°. To evaluate the deformed, recovered and

ACCEPTED MANUSCRIPT

recrystallized grains after grain reconstruction, internal average misorientation angle of each grain was measured. Then, if the average misorientation angle in a grain exceeds the minimum angle of subgrain definition, i.e., 3°, the grain was classified as deformed grain. If internal misorientation was under 3° but the misorientation from one part to other part is above 3° (i.e., grain consist of subgrains) the grain is considered as recovered. All the remaining grains are classified as recrystallized. Coupled thermal-displacement finite element method (Abaqus-dynamic explicit solution) was applied to investigate the variation of stress and temperature in the sample in a 3D model (with mesh type of C3D8T). The materials information in form of impute data are presented in Table 2.

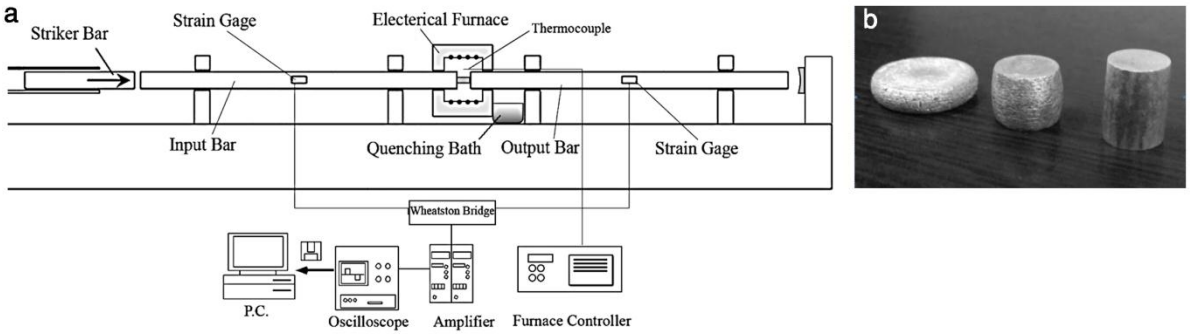

Fig. 1: (a) schematic view of the hot split Hopkinson pressure bar test and (b) initial sample in comparison with two different samples deformed at strain rates of 600 s^{-1} and 1200 s^{-1} at 400°C.

Table 1: Bar information.

d [mm]	A [mm^2]	density [g/mm^3]	E [GPa]	C_o [mm/s]	n
30.00	706.86	7.85×10^{-3}	210	5.172×10^{9}	0.3

Table 2: Materials information used for simulation [17-19].

	Temperature [K]	Density [kg/m^3]	Thermal conductivity [W/mK]	Specific heat[J/gmK]	Elastic modulus [GPa]
Al-Mg	553	2.611×10^{3}	131.6	1.081	58.4
	653	2.589×10^{3}	142.3	1.136	54.8
	753	2.567×10^{3}	152.3	1.178	51.2
	853	2.549×10^{3}	159.5	1.261	47.6
B_4C	553	2.55×10^{3}	24.8	1.481	436.3
	653	2.55×10^{3}	22.4	1.609	430.9
	753	2.55×10^{3}	20.2	1.678	425.5
	853	2.55×10^{3}	18.1	1.686	420.1

3. Result

3.1. Raw data

Generally, in a split Hopkinson pressure bar test, the striker bar hits the input bar that leads to propagation of a compressive uniaxial stress wave through the input bar. At the interface of

ACCEPTED MANUSCRIPT

the sample-input bar, because of impedance mismatching, a fraction of wave transmits through the sample causing deformation of the sample and the other portion of the wave reflects back to the input bar. At the interface of sample-output bar, again, the transmitted wave partially reflects back into the specimen and the remaining fraction transmits to the output bar. As the wave reaches to the free end of the bar, it will reflect back with characteristics related to the free end condition and deforms the sample again. The output of the system is a voltage signal recorded by strain gages on the bars.

Fig. 2a represents a typical signal history recorded from the input and output bars. It is clear that after travelling along the bars and reflecting back from the free ends, the signal shape is distorted. It should be noted that although strain gages record different signals and sample is heavily deformed, only the first signal in input and output bars, which are associated with the first transmitted and reflected wave, have acceptable accuracy for further calculation of strain and stress during deformation.

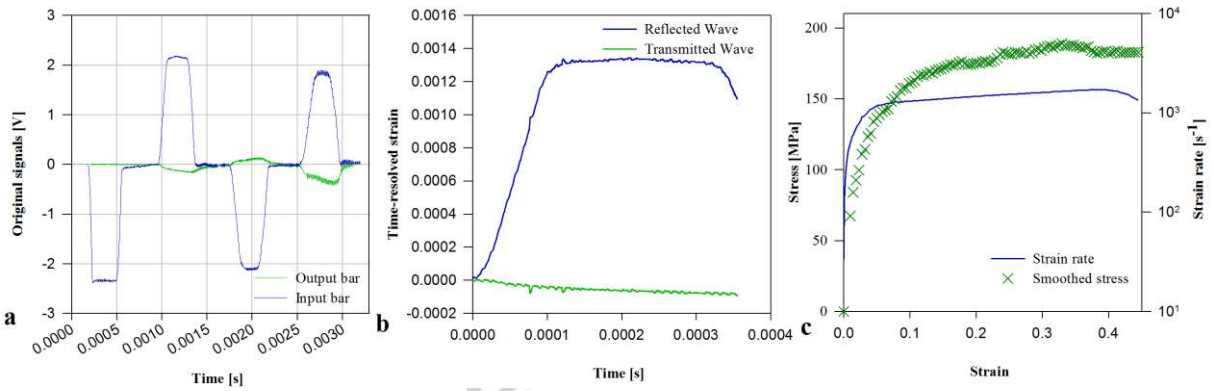

Fig. 2: (a) original input and output signals, (b) first signal in form of time resolved strain vs. time and (c) processed results in form of stress and strain rate vs. strain at 400°C and 1200 s^{-1}.

As shown in Fig. 2b, the signal has to be converted into time-resolved strain based on standard procedure [12]. Finally, the stress and strain rate can be obtained from $\sigma(t) = E_b(A_b / A_s)\varepsilon_T(t)$ and $\dot{\varepsilon}(t) = -2(C_0 / L_s)\varepsilon_R(t)$ as explained in [12], where A and L_s are the initial cross section and length of the specimen, E_b is the Young's modulus of the bar material, $\varepsilon_T(t)$ is the time-resolved strain of the transmitted wave in the output bar of cross-sectional area A_o, $\varepsilon_R(t)$ is the time-resolved strain of the reflected wave in the input bar and C_o is the one dimensional bar wave speed. Strain can be calculated by integration. Then the engineering stress and strain can be converted to true ones. An example of the resulted true stress-strain curve is shown in Fig. 2c.

ACCEPTED MANUSCRIPT

3.2. Data correction

As already mentioned, there are at least three sources of error associated with the resultant stress-strain curves:

(1) Increasing stress resulted from the friction between the specimen and bars. It has been shown that friction reduces velocity components on the surfaces and, by introducing a shear component into the strain rate field, increases the internal power of deformation and therefore the stress. Ebrahimi and Najafizadeh [20] presented a simple applicable method, which by measuring initial and final length (L) and radius (R) of the sample, it is possible to correct the effect of friction according to the following equation:

$$\sigma_{Corrected} = \frac{L\sigma}{8bR}\left(\left(\frac{1}{12}+\left(\frac{L}{Rb}\right)^2\right)^{3/2}+\left(\frac{m}{24\sqrt{3}}\times\frac{\exp(-b/2)}{\exp(-b/2)-1}\right)-\left(\frac{L}{Rb}\right)^3\right)^{-1} \quad (1)$$

where $m=\dfrac{bR_{thory}/L_{final}}{4/\sqrt{3}-2b/3\sqrt{3}}$, $b=4(R_{Midel}-R_{top})\dfrac{L_{final}}{R_{theory}(L_{initial}-L_{final})}$, $R_{thory}=R_{initial}\sqrt{L_{initial}/L_{final}}$, $L=L_{initial}\exp(-\varepsilon)$ and $R=R_{initial}\exp(-\varepsilon/2)$. Here m is a constant friction factor, b is a parameter representing the barreling effect, and L and R are the current ideal length and radius during compression, respectively.

(2) Decreasing stress resulting from adiabatic heating. It is known that a large part of the irreversible plastic work contributes to heat generation, while the rest is stored as strain energy in the form of internal defects. This fact results in an increase in the specimen temperature during the test and so the observed flow stress is lower than the actual one. Accordingly the test cannot be considered under isothermal conditions when no time for dissipation is available, i.e., at high strain rates. Based on the energy balance equation assumptions that were reported and detailed in Hodowany et al. [21], the temperature variations during deformation ($\dot{\theta}$) can be estimated by:

$$\rho c\dot{\theta}=\alpha\eta\sigma\dot{\varepsilon} \quad (2)$$

where ρ is the density of the material, c is the specific heat, α is the fraction of the plastic work dissipated as heat, which is often assumed to be 0.95 for most metals [21], and $\eta=\Delta T_{actual}/\Delta T_{adiabatic}$ is the adiabatic correction factor which is the fraction of adiabatic heat retained in the work piece due to heat loss to the dies. It has been shown that η depends on strain rate under isothermal conditions. For strain rates lower than 0.001 s^{-1}, η is around 0, and under adiabatic conditions and at strain rates greater than 10 s^{-1}, η reaches to 1 [15,21], a value that can be assumed for hot split Hopkinson bar tests. Therefore, the instantaneous

Accepted manuscript

ACCEPTED MANUSCRIPT

temperature can be estimated from Eq. 2. By calculating the deformation heat (δT), at the given strain and strain rate, stress can be corrected by using the variation of stress with respect to temperature, i.e., $\partial\sigma/\partial T$, which in turns can be derived from isothermal tests (i.e., low strain rate tests) or physically based equations

(3) Strain rate corrections. As shown in Fig. 2c, the true strain rate doesn't change from zero to a given value in an instantaneous way. Indeed a significant part of the test is paid in attaining the expected strain rate, and therefore some corrections regarding the stresses associated to this initial part of the curves must be corrected. This can be done by considering the change in strain rate ($\delta\dot{\varepsilon}$), at a given strain and temperature, and the stress can be corrected by using the variation of stress with respect to strain rate, i.e., $\partial\sigma/\partial\dot{\varepsilon}$, which can also be derived from isochronal tests (i.e., low strain rate tests), or from theoretical expressions. Summarizing and applying a linear approximation of multi variable Taylor series, the flow stress curve can be corrected using the following relation:

$$\sigma_{corrected} = \sigma\big|_{\varepsilon.\dot{\varepsilon},T} + \delta T \left.\frac{\partial\sigma}{\partial T}\right|_{\varepsilon,\dot{\varepsilon}} + \delta\dot{\varepsilon} \left.\frac{\partial\sigma}{\partial\dot{\varepsilon}}\right|_{\varepsilon,T} \tag{3}$$

where σ is the friction corrected flow stress at a given T, $\dot{\varepsilon}$ and ε.

3.3. Constitutive analysis

As stated, in order to correct the flow curves according to Eq. 3, it is necessary to find the dependence of stress on temperature and strain rate at a given strain, i.e., a constitutive equation is required. Various theoretical models have been proposed to describe the deformation behavior of metals at high temperatures. Most of them distinguish between low and high stacking fault energy (SFE) materials [22]. Based on the value of SFE of Al-Mg alloys, dynamic recovery is the most important softening mechanism active, especially at high strain rates [23]. Bergstrom [24] proposed a model for metals undergoing exclusively dynamic recovery which has been developed by Laasraoui and Jonas [25] and Lin et al. [26] based on a balance between the hardening and the softening mechanisms due to the dislocation multiplication and the annihilation during deformation respectively. According to this model, the dislocation density ρ depends on strain as follows:

$$\frac{d\rho}{d\varepsilon} = U - \Omega\rho,\ \varepsilon = 0 \rightarrow \rho = \rho_o \text{ and } \varepsilon = \infty \rightarrow \rho = \rho_{rec} \tag{4}$$

ACCEPTED MANUSCRIPT

where U and $\Omega\rho$ represent the strain hardening and dynamic recovery terms, ρ_o is the dislocation density before starting deformation, and ρ_{rec} is the equilibrium dislocation density achieved at large strains. Assuming strain-independency of U and Ω, and using the classic relationship between stress and dislocation density, $\sigma = \alpha Gb\sqrt{\rho}$, ($\alpha$ is a constant, G is the shear modulus, and b the burgers vector) the above differential equation can be solved and rewritten as:

$$\sigma^2 = \sigma_{rec}^2 + (\sigma_{rec}^2 - \sigma_o^2)\exp(-\Omega\varepsilon) \tag{5}$$

where σ is the flow stress, $\sigma_o = \alpha Gb\sqrt{\rho_o}$ and $\sigma_{rec} = \alpha Gb\sqrt{U/\Omega}$ are the yield stress and the saturation stress due to dynamic recovery, respectively. It is worth mentioning that at high temperature conditions yield stress can be ignored compared with the saturation stress. For description of saturation stress as a function of strain rate and temperature, different equations have been proposed [25-28]. In hot deformation studies, it is common to consider the combined effects of temperature and strain-rate on a single parameter, i.e., the so-called Zener–Hollomon (Z) parameter [29]. In the high strain rate regime it is accepted that Z has an exponential dependence on stress as follows [30]:

$$Z = \dot{\varepsilon}\exp(Q/RT) = A\exp(\beta\sigma/G) \tag{6}$$

where Q is the activation energy for deformation which in the present alloy can be considered equal to 145 kJ/mol [31], G the shear modulus, which in turns depends on temperature (for Al-Mg alloy, this dependency can be expressed as: $G = 78427 - 36.18T$ [32]), and A and β are constant which can be calculated from experimental results. Finally, the softening term, Ω, dependence on temperature can also be expressed as [27]:

$$\Omega = kZ^n \tag{7}$$

where, k and n are material constant. Therefore, the dependence of flow stress on deformation conditions (i.e., on the Zener Hollomon parameter) due to dynamic recovery at high temperature deformation can be written as follows:

$$\sigma = \left\{\left(\frac{1}{\beta}\left(\ln Z - \ln A\right)\right)^2 (1 - \exp(-kZ^n\varepsilon))\right\}^{0.5} \tag{8}$$

Considering friction corrected curves (Fig.3a), saturation stress can be obtained as the stress at which the hardening rate ($\theta = \partial\varepsilon/\partial\sigma$) is equal to zero in a θ-σ plot (Fig. 3b). Based on Eq. 5, the softening factor, Ω, can be calculated by representing $-\ln(1-(\sigma/\sigma_{rec})^2)$ versus ε

(Fig.3c). In order to find material constants in Eq. 8, partial differentiation of Eq. 6 and Eq. 7 must be done, i.e., $\partial \ln \dot{\varepsilon} / \partial(\sigma / G)\big|_T$ and $\partial \ln \Omega / \partial \ln Z$ that yield β and n values. In turns, by plotting $\ln Z$ with respect to $\beta\sigma / G$ and $\ln \Omega$, the parameters A and k can be obtained, respectively.

It should be noted that both the deformation heat and strain rate corrections use the developed constitutive equation, which are obtained from uncorrected data; hence, constants in Eq. 8 should be renewed according to the new curve. This procedure can be continued until negligible stress variation is obtained after some cycles. The curve correction sequences are presented in Fig. 4a, and as shown in Fig. 4b after the third cycle calculation, the stress obtained is already steady and the error is negligible. Therefore, this level of stress was considered as the final corrected stress. An example of these procedures is shown in Fig. 4c.

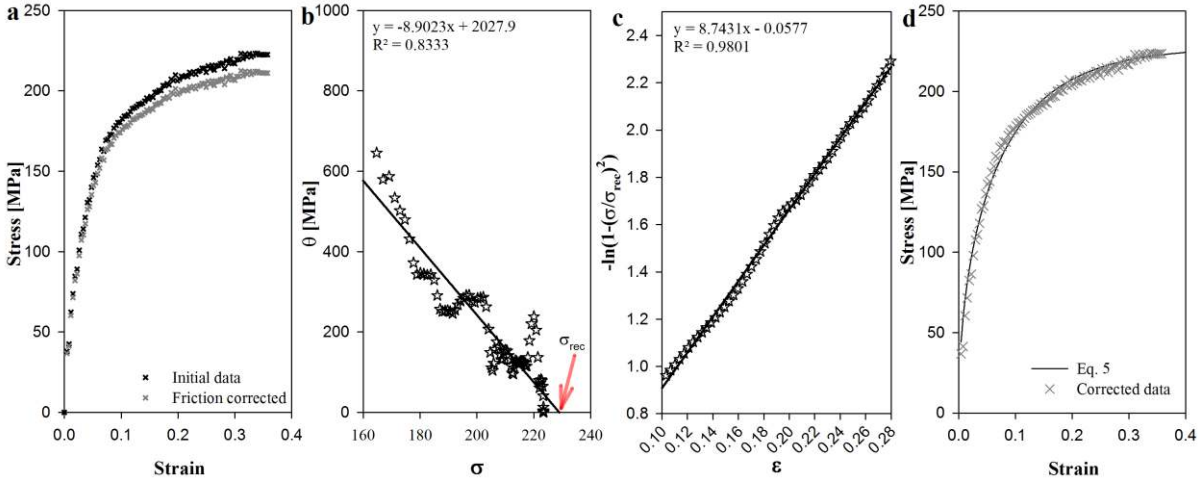

Fig. 3: (a) correction steps on original data of Al-3Mg deformed at 300°C in strain rate of 1000 s^{-1}, (b) finding saturation recovery stress σ_{rec} and (c) softening coefficient Ω by linier regression, and (d) comparing experimental data vs. output of $\sigma = \{\sigma_{rec}(1-\exp(-\Omega\varepsilon))\}^{0.5}$.

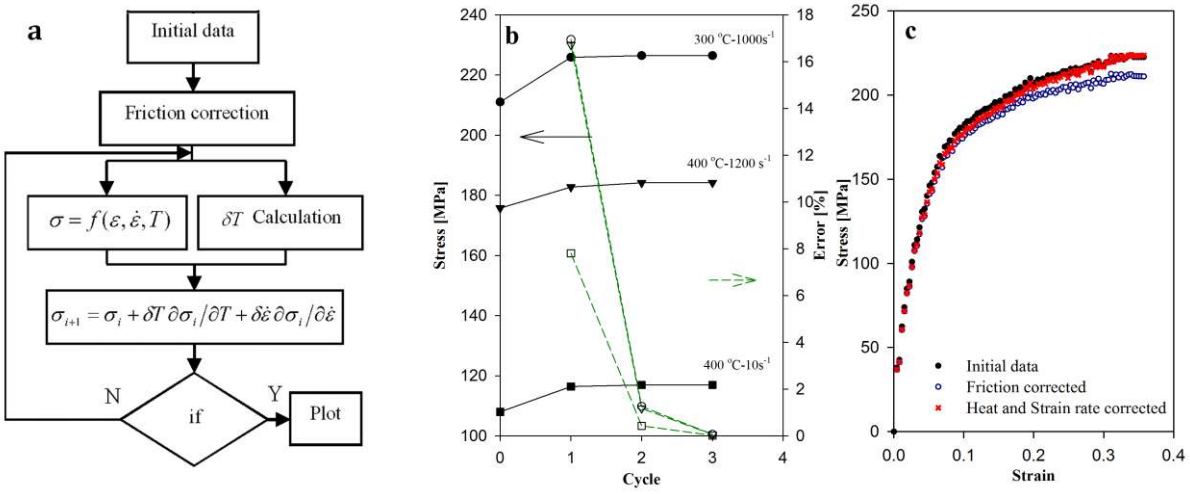

Fig. 4: (a) flow curve correction algorithm, (b) variation of stress in different cycles of correction, and (c) different corrections on initial curve (300°C and 1000 s^{-1}).

All results including Al-3Mg and Al-Mg/B_4C composite flow curves were corrected with presented method and are shown in Fig. 5. According to this figure, Al-Mg/B_4C composite, and as expected, have higher flow stress in different deformation conditions than the single phase alloy. In both materials rising temperature and decreasing strain rate resulted in lowering of the strength. Fig. 6 represents the constitutive analysis for both Al-3Mg alloy and Al-3Mg/10%vol. B_4C composite to find constants in Eq. 8. They are reported in Table 3. According to Fig. 7, predicted flow curves obtained from Eq. 8 have good agreement with experimental results.

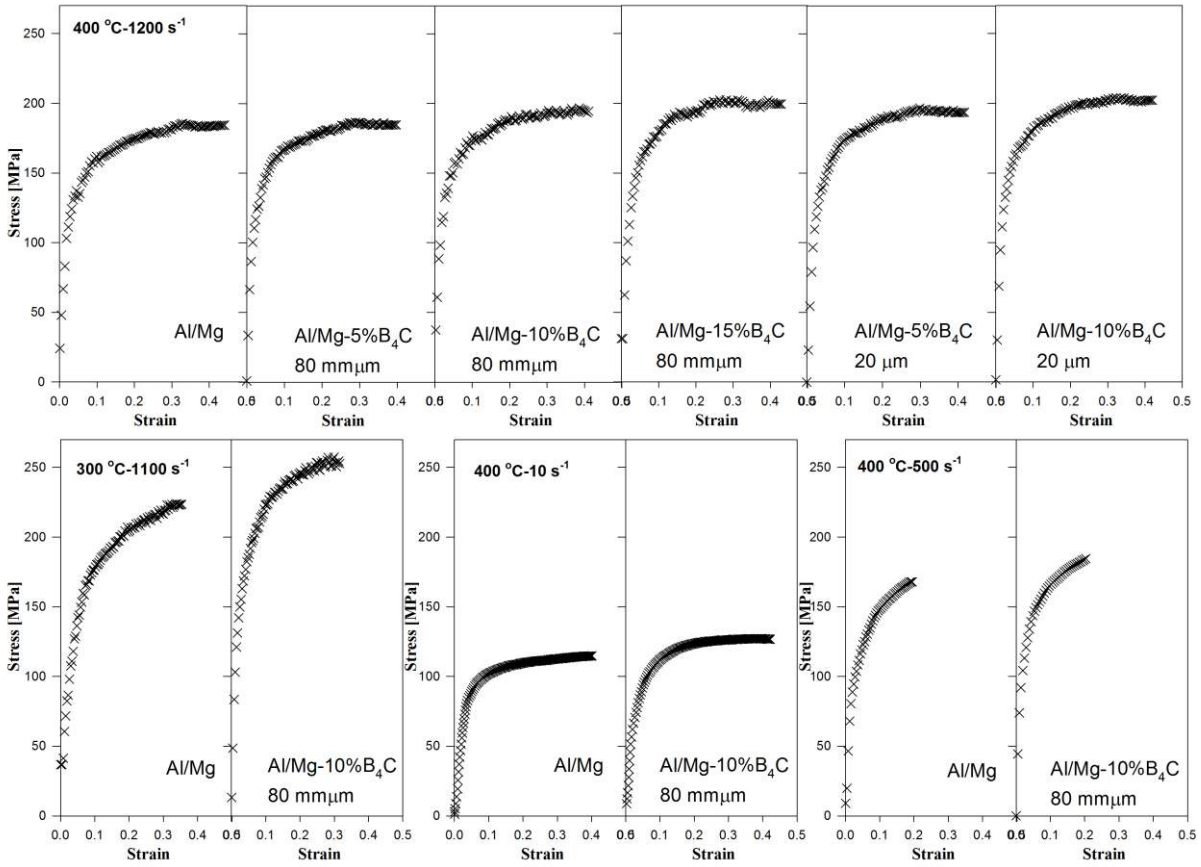

Fig. 5: Flow curves of Al-3Mg and various Al-3Mg/B_4C composites with particle size of (80 and 20 μm) after correction for different deformation conditions.

ACCEPTED MANUSCRIPT

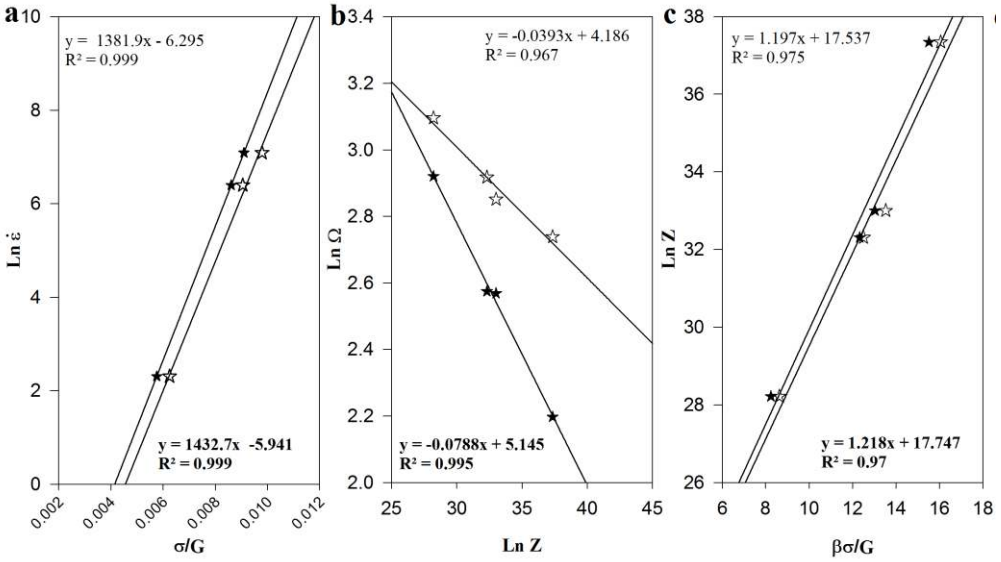

Fig. 6: Constitutive analyses for Al-3Mg (solid symbol) and Al-3Mg/10%vol.B_4C (open symbol)), to obtain value of (a) modified stress multiplier β, (b) n and k for softening coefficient, and (c) A.

Table 3: constants in Eq. 8 for Al-Mg and Al-3Mg/10vol.% B_4C composite.

Material	A	β	k	n
Al-3Mg	17.75	1432.7	171.6	0.08
A-3Mg/ 10% vol.B_4C	17.54	1381.9	64.79	0.04

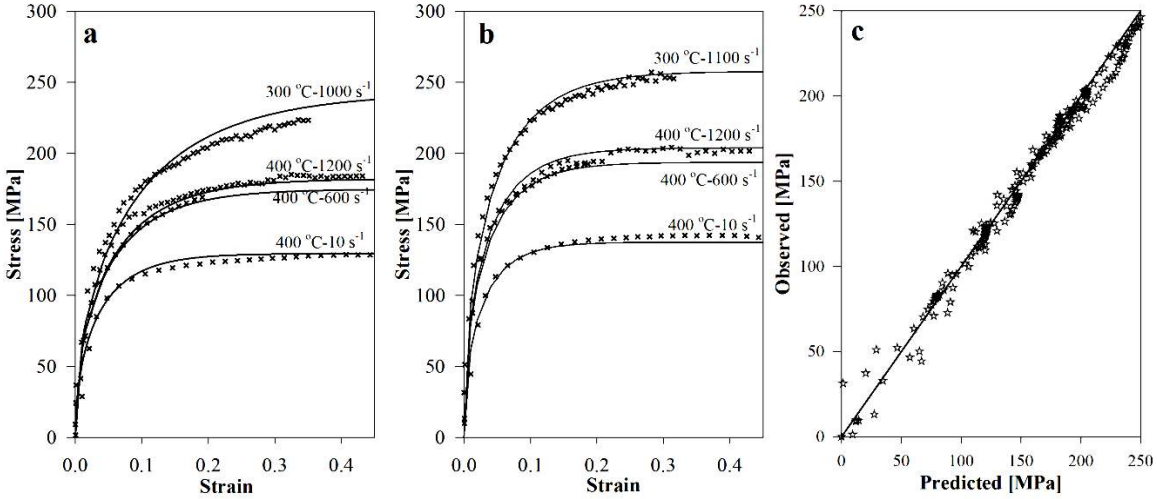

Fig. 7: Flow curves of Al-3Mg (a) and Al-3Mg/10 vol.% B_4C composites (b) after correction according (symbols) and predicted flow curves based on developed constitutive equation (lines) and (c) predicted values vs. experimental data.

4. Discussion

The flow curves of the composite material in comparison with the single phase alloy have higher hardening rate which is followed by more softening before stress saturation as shown in Figs. 7a, b. This phenomenon can be identified clearly by comparing their softening factors

ACCEPTED MANUSCRIPT

for different Z. According to Fig.6b, the softening factors of the flow curves in the composite material are higher than those of the single phase alloy, especially at higher values of *Z*, i.e., high strain rates and low temperatures. Moreover, the calculation of the softening factor for the composite material with different volume fractions of reinforcement reveals that softening is promoted by increasing particles fraction (Fig. 8a). Composites reinforced with finer particles, at the same volume fraction, displays lower softening factor. Based on θ-ε curves which are obtained from the developed constitutive equation (Fig. 8b), at initial strains, i.e., less than 0.1, hardening rate in composite materials is higher than in the single phase counterpart alloy and then it is gradually decreasing to lower values than in the single phase alloy.

In composites reinforced with large particles, the main strengthening mechanism is load transferred from matrix to hard particles [1] which in turn leads to form stress gradient from particle to matrix which will be relaxed by geometrically necessary dislocation in low strains. Increase in deformation will lead to appearance of deformation zone (DZ) around particles with high dislocation density and large misorientation gradient. By increasing the volume fraction of reinforcement, the probability of overlapping these areas will also increase which leads to formation of heavily deformed areas containing rotated and fractured work hardened grains [6,33]. As a result, the matrix will show higher hardening rate during straining.

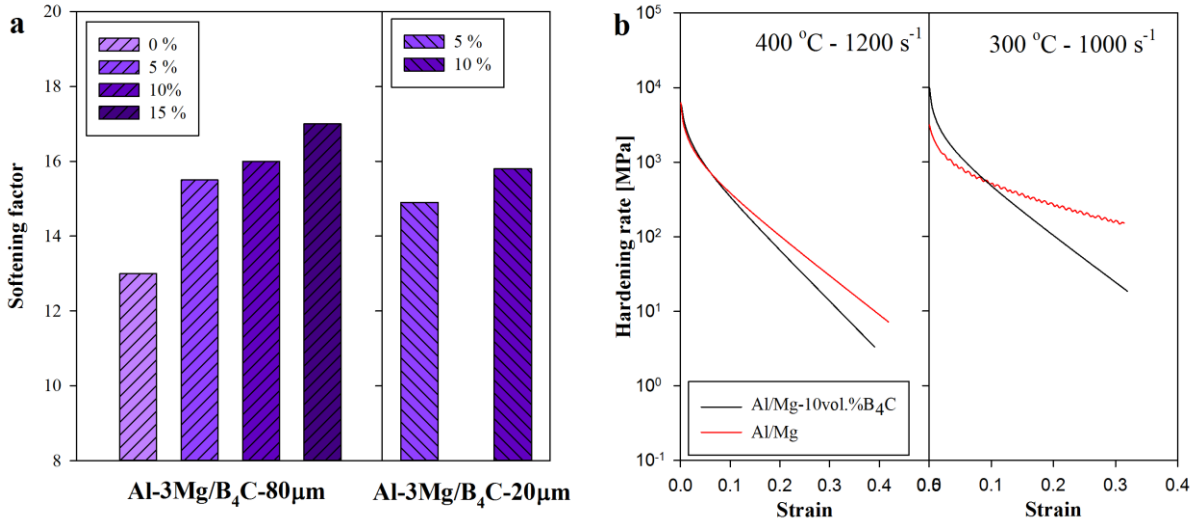

Fig. 8: a) Variation of softening factor with Z for different volume fraction of reinforcement and b) variation of hardening rate via strain in Al-3Mg and Al-3Mg/B_4C for different deformation condition.

Fig. 9 represents the EBSD micrographs of Al-Mg/B_4C composite deformed at 400˚C with strain of 0.7, 0.46 and 1.28 and strain rate of 10 s^{-1}, 600 s^{-1} and 1200 s^{-1}, respectively. As it can be seen, the microstructure contains low angle boundaries bordered by high angle

ACCEPTED MANUSCRIPT

boundary. Deformation zone, where work hardened grains were formed, are located in the compression direction (Y direction). Although at low strain or strain rate (Fig. 9a, b) the microstructure contains several recovered grains, grains in DZ areas are highly missoriented and are classified as work hardened. At higher deformation values, up to a strain of 1.28 (Fig. 9c, d), to the appearance of some recrystallized fine grains (white grains) in the microstructure mainly concentrates around particles. Far away from particles, in the matrix, also some recrystallized grains can be occasionally identified, while most of grains in this area are deformed or recovered. Moreover, as shown in Fig. 10a, in heavily deformed zones the microstructure is formed by elongated and in some cases fractured grains. In all of three cases, large numbers of low angle grain boundaries are developed in the microstructure as a result of the dislocation generation and annihilation mechanisms (dislocation climb and cross slip) (Fig. 9e). Therefore, based on the appearance of the deformation zones, reinforced matrix contains more hardened grains which result in higher hardening rate; however, considering the softening factor and flow curves, composite materials show less hardening during large deformation.

Two groups of softening mechanisms can be identified in the flow curve for the softening of the present composites materials, namely (A) direct mechanisms, which relate to microstructure evolution of matrix, and (B) indirect mechanisms, which relate to limitation in strengthening mechanisms.

A) Direct softening. Occurrence of dynamic recovery (DRV), dynamic recrystallization (DRX), texture softening and particles orientation rearrangement are known as the main flow softening mechanisms. Although it is well known that in aluminum alloys, high temperature deformation is associated with dynamic recovery [34], according to Fig. 9f the fraction of recovered grains are reduced by increasing strain rate (from 10 s^{-1} to 600 s^{-1}) while softening is enhanced in flow curves by increasing strain rate. Hence, DRV is not the only reason of softening.

Accepted manuscript

ACCEPTED MANUSCRIPT

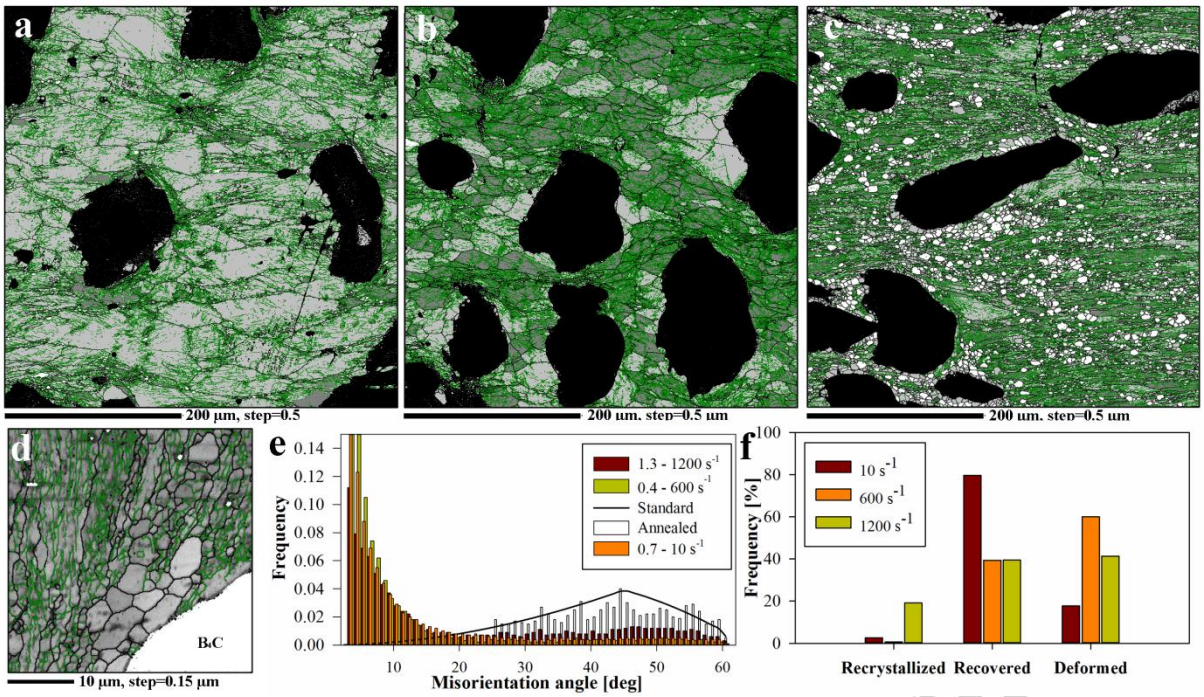

Fig. 9: EBSD micrographs of Al-3Mg/10 vol.% B_4C deformed at 400°C with strain and strain rate of (a) 0.7 and 10 s^{-1} (b) 0.46 and 600 s^{-1}, (c and d) 1.28 and 1200 s^{-1}, (e) corresponding grain boundary misorientation variation and (f) fraction of hardened, recovered and recrystallized grains. Black area: B_4C particles, dark gray: deformed grains, light gray: recovered grains, white: recrystallized grains and green line: low angle boundaries and compression direction is Y direction.

It has been reported that at high strain rate deformation, strain and consequently dislocation arrays have inhomogeneous distribution in structure which in turn provides appropriate sites for nucleation of new grains during deformation [35]. Therefore, one may consider the presence of small recrystallized grains in microstructure due to DRX. However, considering the high value of *Z* parameter, the occurrence of DRX even promoted by particle stimulated nucleation (PSN) is not probable. Moreover, at strain rate of 10 s^{-1}, which is more suitable for PSN, fewer recrystallized grains are observed in comparison with strain rate of 1200 s^{-1} (Fig. 9f). It has been mentioned that Al-3Mg alloy are very sensitive to static recrystallization (SRX) just after hot deformation, even in short quenching times [35]. For this reason different equations have been developed for obtaining critical time for occurrence of 50% SRX ($t_{0.5}$) after deformation [36,37]. Based on these equations, $t_{0.5}$ for deformation at 400°C with 1200 s^{-1} up to 1.28 is less than 0.1 s and for deformation at 400°C with 600 s^{-1} up to 0.46 is less than 0.7 s. Hence, the happening of SRX just after finishing of deformation is reasonable.

At high strains, more than 2, new recrystallized grains can be formed from continuous fragmentation of elongated serrated grains which is also named geometrical dynamic recrystallized (GDRX) [35,39]. It has been reported that Al-3Mg alloy can be subjected to

ACCEPTED MANUSCRIPT

Meta Dynamic recrystallization (MDRX) – the one that follows to GDRX - just after deformation, especially for high value of *Z* [38]. Some examples of these grains are shown in Fig. 10d. It should be noted that the overall strain of sample is less than 2, but local strain in deformation zones, as it is presented in Fig. 10b, can exceed from 3 and the strain condition are therefore suitable for GDRX to take place. To distinguish between these two types of recrystallizations, one can compare the grain orientation of new grains with deformed grains. It is accepted that GDRXed grains have strong relation with original grains, while, SRXed grains have different texture in comparison with deformed grains. Fig. 10e represents two pole figures from different areas, namely, vicinity of particle which mainly contains recrystallized grains and matrix far away from particles which is mainly formed by deformed and recovered grains. As it can be seen, matrix far away from particles shows a strong {110} fiber; however, recrystallized grains show a random orientation. Therefore it can be concluded that new grains are statically recrystallized in heavily deformed area and they cannot improve the softening rate in composites.

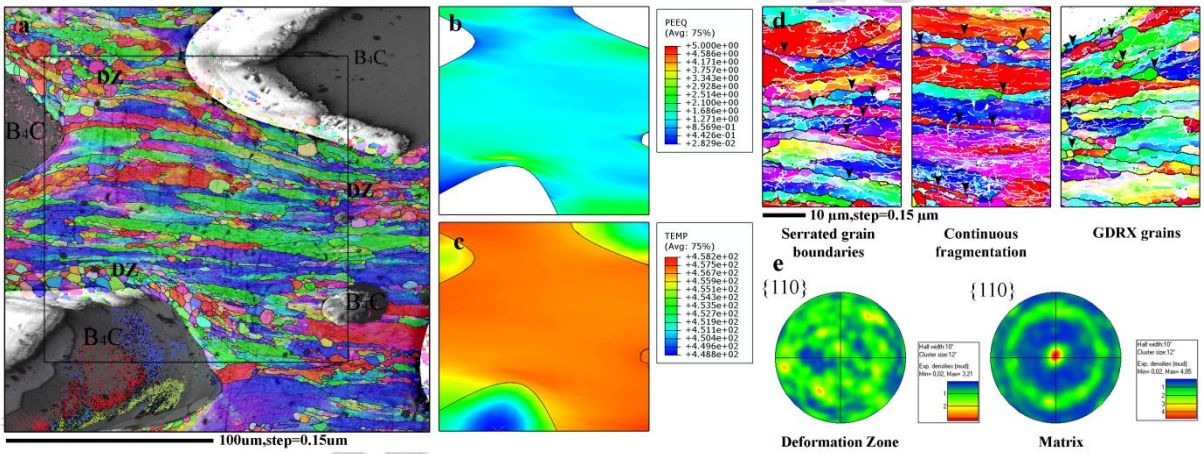

Fig. 10: (a) EBSD map from the vicinity of B_4C particles deformed at 400°C with strain rate of 1200 s^{-1}, (b) FEM simulation of strain and temperature variation for selected area, (c, b) formation of GDRXed grains and (e) {110} pole figures for microstructure around particles and matrix far away from particles.

Considering the facts that the hardening rate will be reduced during GDRX [40] and grain refinement happened during deformation around particle in composites, it is reasonable that the overall hardening rate of composite is lower than the single phase alloy. This phenomenon is directly related to the deformation zone size which it in turn is a function of volume fraction and size of particles. Fig. 11 represents the microstructure of composite with smaller particles (<20µm). One can notice that there are few SRXed and GDRXed grains around the particles. It is because the initial size of grains is relatively equal to particle size and therefore, deformation zone around a particle will not consist more than one grain (Fig.

ACCEPTED MANUSCRIPT

11c). As already mentioned, at large deformation, the occurrence of GDRX can reduce the hardening rate; however, based on flow curves, even for low value of strains (0.2-0.4) where there is no sign of GDRX (Fig. 9a, b) composites show lower hardening rate in both particle sizes than single phase alloy.

Considering the particles morphology (particles aspect ratio ~ 1) the particles rearrangement due to matrix flow can be ignored. Besides, based on the fact that PSN did not happened, presence of particles in matrix cannot significantly influence the texture. Therefore, the direct softening mechanisms do not have significant impact on softening observed in flow curves.

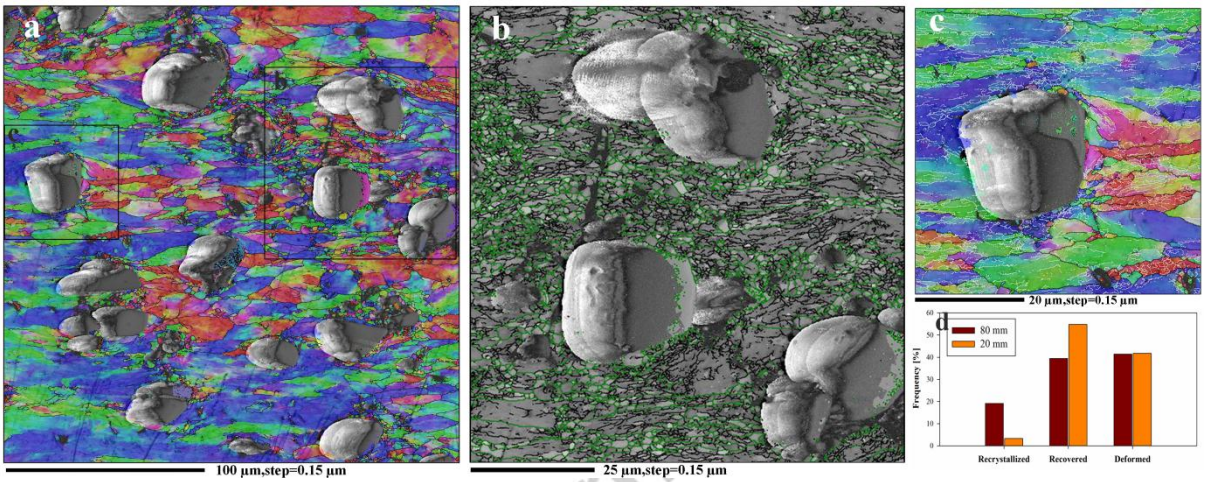

Fig. 11: (a-c) EBSD micrographs of Al-3Mg/10 vol.% B_4C composite deformed at 400°C with strain and strain rate of 1.28 and 1200 s^{-1} respectively, (d) fraction of recrystallized, recovered and hardened grains for Al-3Mg/10 vol.% B_4C composites with different particle size.

B) Indirect softening. There is also another important mechanism which reduces the hardening rate, i.e., limiting load transfer mechanism. It has been known that during plastic deformation of composite materials, relaxation processes, including atomic diffusion, recovery and rearrangement of dislocations, grains recrystallization, interfacial sliding and particle fracture, lower the internal strain energy and lead to decrease in the hardening rate [1]. Considering the rate of deformation in the present study and the particle-matrix interface situation in the present material [16], atomic diffusion and interfacial sliding can be ignored. Moreover, as discussed in previous sections, DRX cannot occur during deformation. However, based on microstructure observation, particle fracture is possible.

According to secondary electron micrographs, Fig. 12, some of particles are fractured during deformation. It has been reported that fracture of particles can reduce load transfer mechanism [41,42]. Nan and Clarke [42] mentioned that a fractured particle acts as a hole in matrix so during straining, the occurrence of particle fracture reduces the flow stress to

ACCEPTED MANUSCRIPT

$(f-1)$ times of matrix flow stress, where f is the volume fraction of particles. The fracture strength of particles is related to their diameter, D, i.e., $\sigma_f = K_{IC}/\sqrt{D}$. Therefore, as Abedini and Chen mentioned [41], more particles (ξ) will be fractured during deformation of composite reinforced with bigger particles, i.e., $\xi = \exp[\sigma_P/\sigma_f]^m$, where σ_P is the stress transferred to particle. It can also be proved from Fig. 8 by comparing the numbers of fractured particles in micrographs. This phenomena, in turn, leads to the appearance of lower hardening rate during straining. Increasing Z parameter leads to enhance flow stress which consequently raises the load transferred to particles. In turn, it will increase the probability of particle fracture. As a result by increasing strain rate and reducing deformation temperature, hardening rate will be more reduced, or in other words, softening rate will be enhanced, as observed in experimental results (Fig. 8).

Deformation at such high strain rates leads to increase the matrix temperature due to adiabatic heating. Based on the load transfer mechanism, matrix of composite in comparison with single phase alloy, experiences more strain in equal deformation condition [43]. Therefore the rising of temperature in the matrix is higher with respect to single phase alloy. Based on simulation results, the average strain in the matrix (1.56) is 1.22 times larger than the average strain of the single phase alloy (1.28). According to the adiabatic heating equation (Eq.2), such higher strain in matrix will result in 22% more heat of deformation. Therefore, considering the sensitivity of aluminum strength to temperature ($\partial\sigma/\partial T$), the difference in deformation temperature of matrix and single phase alloy leads to different in hardening as observed. Hence, appearance of lower hardening rate in composite flow curves are mainly related to limiting load transfer mechanism based on particle fractures and higher adiabatic heating in matrix.

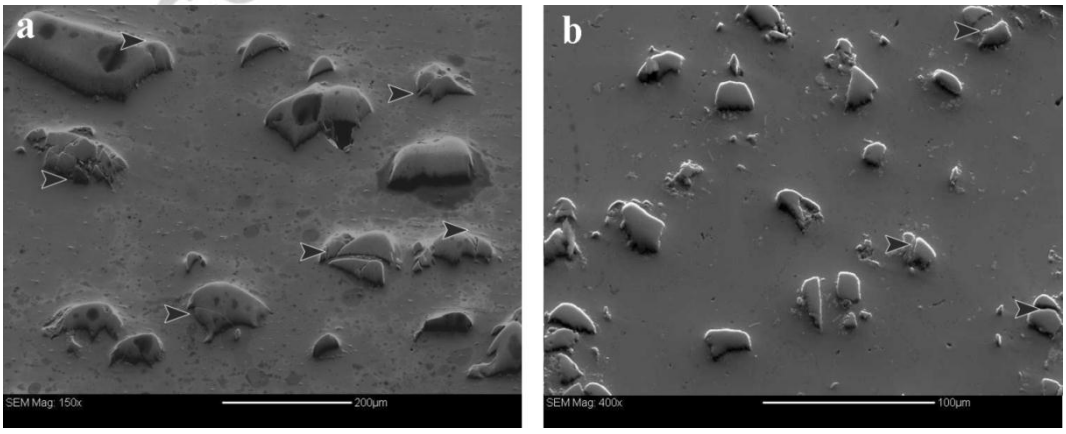

Fig. 12: Secondary electron micrographs of Al-3Mg/10vol.%B_4C with particle size of (a) 80 and (b) 20 µm, deformed at 400°C with strain and strain rate of 0.46 and 600 s^{-1} respectively.

ACCEPTED MANUSCRIPT

Conclusion

Al-3Mg alloy and Al-3Mg/B_4C composite in different volume fractions and particle sizes were deformed at high strain rates (from 10 to 10^3 s^{-1}) at elevated temperatures. To correct the effects of friction, adiabatic heating and strain rate variation during deformation on initial outputs, a pre-processing method was presented. Moreover, a physically based method was successfully applied to model the dynamic deformation responses in form of stress flow curves. It was observed that composite materials in comparison with single phase alloy show higher hardening rate at initial strains, followed by higher level of softening before stress saturation. This phenomenon, higher softening rate in composites, was intensified by increasing volume fraction of reinforcement and particle size. Microstructural investigation revealed that although geometrical dynamic recrystallization happened in deformation zones around particles, softening was mainly related to imperfect load transfer mechanism due to particle fracture during deformation.

References

[1] T.W. Clyne and P.J. Withers, An introduction to metal matrix composites, Cambridge University Press, 1995.

[2] C.M. Sellars and W.J.M. Tegart, "Hot Workability", *International Metallurgical Reviews*, vol. 17, 1972, pp. 1-24.

[3] H.J. McQueen and I.Poschmann2"Subgrain development in hot working of Al and Al-5Mg", *Materials Science and Engineering A* vol. 234–236, 1997, pp. 830-833.

[4] I. Poschmann and H.J. McQueen, "Flow softening and microstructural evolution of al-5mg during hot working"," *Scripta Materialia*, vol. 35, 1996, pp. 1123-1128.

[5] C.S. Ramesh, R. Keshavamurthy, P.G. Koppad and K.T. Kashyap, "Role of particle stimulated nucleation in recrystallization of hot extruded Al6061/SiC_p composites", *Transactions of Nonferrous Metals Society of China*, vol. 23, 2013, pp. 53-58.

[6] F.J. Humphreys, "The thermomechanical processing of A1-SiC particulate composites", *Materials Science and Engineering A*, vol. 135, 1991, pp. 267-273.

[7] H. Li, H. Wang, M. Zeng, X. Liang and H. Liu, "Forming behavior and workability of 6061 / B 4 C P composite during hot deformation", *Composites Science and Technology*, vol. 71, 2011, pp. 925-930.

[8] J.C. Shao, B.L. Xiao, Q.Z. Wang, Z.Y. Ma, Y. Liu and K. Yang, "Constitutive flow behavior and hot workability of powder metallurgy processed 20 vol .% SiC/2024Al composite", *Materials Science and Engineering A*, vol. 527, 2010, pp. 7865-7872.

[9] G.T. S I HongGray and J.J. Lewandowski, "Dynamic deformation behavior of Al-Zn-Mg-Cu alloy matrix composites reinforced with 20 vol.% SiC", *Acta Materialia*, vol. 41, 1993, pp. 2337-2351.

Accepted manuscript

ACCEPTED MANUSCRIPT

[10] H. Zhang, K.T. Ramesh and E.S.C. Chin, "High strain rate response of aluminum 6092 / B4C composites", *Materials Science and Engineering A*, vol. 384, 2004, pp. 26-34.

[11] J. Shim and D. Mohr, "Using split Hopkinson pressure bars to perform large strain compression tests on polyurea at low , intermediate and high strain rates", *International Journal of Impact Engineering*, vol. 36, 2009, pp. 1116-1127.

[12] W.W. Chen and B. Song, Split Hopkinson Bar, Design, Testing and Applications, Springer, 2011.

[13] S. Seo, O. Min and H. Yang, "Constitutive equation for Ti – 6Al – 4V at high temperatures measured using the SHPB technique", *International Journal of Impact Engineering*, vol. 31, 2005, pp. 735-754.

[14] M. Sedighi, M. Khandaei and H. Shokrollahi, "An approach in parametric identification of high strain rate constitutive model using Hopkinson pressure bar test results", *Materials Science and Engineering A*, vol. 527, 2010, pp. 3521-3528.

[15] J. Kajberg and K. Sundin, "Material characterisation using high-temperature Split Hopkinson pressure bar", *Journal of Materials Processing Technology*., vol. 213, 2013, pp. 522-531.

[16] M. Rezayat, M.R. Bahremand, M.H. Parsa, H. Mirzadeh and J.M. Cabrera, "Modification of As-cast Al-Mg/B_4C composite by addition of Zr", *Journal of Alloys and Compounds*, vol. 685, 2016, pp. 70-77.

[17] S. Ramana Murthy, "Elastic properties of boron carbide", *Journal of Materials Science Letters*, vol. 4, 1985, pp. 603-605.

[18] S.P. Dodd, G.A. Saunders, C. Lane, and S.K.T. Oee, "Temperature and pressure dependences of the elastic properties of ceramic boron carbide (B_4C)", *Journal of Materials Science*, vol. 37, 2002, pp. 2731 - 2736.

[19] E.A. Brandes and G.B. Brook, Smithells Metals Reference Book, Butterworth Heinemann, 1992.

[20] R. Ebrahimi and A. Najafizadeh, "A new method for evaluation of friction in bulk metal forming", *Journal of Materials Processing Technology*, vol. 152, 2004, pp. 136-143.

[21] J. Hodowany, G. Ravichandran, A.J. Rosakis and P. Rosakis, "Partition of plastic work into heat and stored energy in metals", *Experimental Mechanics*, pp. 113-123.

[22] Y.C. Lin and X.M. Chen, "A critical review of experimental results and constitutive descriptions for metals and alloys in hot working", *Materials and Design*, vol. 32, 2011, pp. 1733-1759.

[23] H.J. McQueen and I. Poschmann, "Subgrain development in hot working of Al and Al-5Mg", *Materials Science and Engineering A*, vol. 234, 1997, pp. 830-833.

[24] Y. Bergstrom, "A dislocation model for the strain-ageing behaviour of steel", *Materials Science and Engineering*, vol. 9, 1972, pp. 101-110.

[25] A. Laasraoui and J.J. Jonas, "Prediction of steel flow stresses at high temperatures and strain rates", *Metallurgical Transactions*, vol. 22, 1991, pp. 1545-1558.

[26] Y.-cheng Lin, M.-song Chen and J. Zhang, "Modeling of flow stress of 42CrMo steel under hot compression", *Materials Science and Engineering A*, vol. 499, 2009, pp. 88-92.

[27] S. Serajzadeh and A.K. Taheri, "An investigation of the silicon role on austenite recrystallization", *Materials Letters*, vol. 56, 2002, pp. 984 - 989.

Accepted manuscript

ACCEPTED MANUSCRIPT

[28] J.R. Cho, W.B. Bae, W.J. Hwang and P. Hartley, "A study on the hot-deformation behavior and dynamic recrystallization of Al ± 5 wt .% Mg alloy", *Journal of Materials Processing Technology*, vol. 118, 2001, pp. 356-361.

[29] H. Hollomon, C. Zener, C. Zener and H. Hollomon, "Effect of Strain Rate upon Plastic Flow of Steel", *Journal of Applied Physics*, vol. 15, 1943, pp. 22-32.

[30] H. Mirzadeh, J. Maria and A. Najafizadeh, "Constitutive relationships for hot deformation of austenite", *Acta Materialia*, vol. 59, 2011, pp. 6441-6448.

[31] H.J. Mcqueen and N.D. Ryan, "Constitutive analysis in hot working", *Materials Science and Engineering A*, vol. 322, 2002, pp. 43 - 63.

[32] R. Carmona, Q. Zhu, C.M. Sellars and J.H. Beynon, "Controlling mechanisms of deformation of AA5052 aluminium alloy at small strains under hot working conditions", *Materials Science and Engineering A*, vol. 393, 2005, pp. 157-163.

[33] F.J. Humpherys and P.N. Kalu, "Dislocation-particle interactions during high temperature deformation of two-phase aluminium alloys", *Acta Metallurgica*, vol. 35, 1987, pp. 2815-2829.

[34] H.J. Mcqueen, "Recent advances in hot working: fundamental dynamic Softening mechanisms", *American Society for Metals*, vol. 3, 1984.

[35] F.J. Humphreys and M. Hatherly, Recrystallization and related annealing phenomena, Elsevier, 2004.

[36] M.A. Zaidi and T. Sheppard, "Recrystallization kinetics of AI-Mg alloys AA 5056 and AA 5083 after hot deformation", *Materials Science and Technology*, vol. 2, 1986, pp. 938-945.

[37] M.A. Wells, D.J. Lloyd, I.V. Samarasekera, J.K. Brimacimbe and E.B. Hawbolt, "Modeling the microstructural changes during hot tandem rolling of AA5XXX aluminum alloys: part I. Microstructural evolution", *Metallurgical and Materials Transactions B*, vol. 29, 1998, pp. 611-620.

[38] J.K. Chang, K. Takata, K. Ichitani and E.M. Taleff, "Abnormal grain growth and recrystallization in Al-Mg Alloy AA5182 following hot deformation", *Metallurgical and Materials Transactions A*, vol. 41, 2010, pp. 1940-1953.

[39] W. Blum, Q. Zhu, R. Merkel and J. Mcqueen, "Geometric dynamic recrystallization in hot torsion of A1-5Mg-0.6Mn", *Materials Science and Engineering A*, vol. 205, 1996, pp. 23-30.

[40] M. Rezayat, A. Akbarzadeh, "Fabrication of aluminium matrix composites reinforced by submicrometre and nanosize Al_2O_3 via accumulative roll bonding", *Materials Science and Technology, vol. 28, 2012, pp. 1233-1240.*

[41] A. Abedini and Z.T. Chen, "A micromechanical model of particle-reinforced metal matrix composites considering particle size and damage", *Computational Materials Science*, vol. 85, 2014, pp. 200-205.

[42] C.W. Nan and D.R. Clarke, "The influence of particle size and particle fracture on the elastic/plastic deformation of metal matrix composites", *Acta Materialia*, vol. 44, 1996, pp. 3801-3811.

[43] G.P. Tandon and G.J. Weng, "A theory of particle-reinforced plasticity", *Journal of Applied Mechanics*, vol. 55, 1988, pp. 126-135.

Accepted manuscript